Available online at www.sciencedirect.com
SCIENCE DIRECT®
International Journal of Heat and Mass Transfer 47 (2004) 3783–3795
International Journal of HEAT and MASS TRANSFER
www.elsevier.com/locate/ijhmt

Some unexpected effects of wavelength and perturbation strength on heat transfer enhancement by Görtler instability

Ladan Momayez, Pascal Dupont, Hassan Peerhossaini *

Laboratoire de Thermocinétique, CNRS UMR 660 7, École polytechnique de l'Université de Nantes, La Chantrerie, BP 50609, Nantes, F-44306, France

Received 2 September 2003; received in revised form 18 March 2004

Abstract

Convective heat transfer is studied in a laminar boundary layer over a concave wall in the presence of Görtler vortices with constant wall heat flux conditions. Comparison of local Nusselt and Stanton numbers demonstrates that the latter is more accurate in revealing three-dimensional flow development. Analysis of heat transfer with different freestream velocities shows that the Reynolds similarity is not valid in the presence of Görtler centrifugal instability and indicates that the Görtler number based on the Blasius momentum thickness enables one to follow the different steps of Görtler instability development. Analysis of the effects of the Görtler vortex wavelength and of perturbation wire diameter shows that the smaller the vortex wavelength, the faster the apparent transition to turbulence. Moreover, larger wire diameters also cause a faster boundary-layer transition.

It has been shown experimentally that in the range of heat loading studied here, the buoyancy force has no effect on Görtler vortex generation and growth.

1. Introduction

The boundary-layer transition on a concave wall is complicated by the presence of a centrifugal instability phenomenon called Görtler instability resulting from an imbalance between the centrifugal force and the radial pressure gradient. The Görtler number G_θ indicates the relative influence of centrifugal and viscous forces on fluid particle motion, where θ is the Blasius momentum thickness. Even though Hall [1] has demonstrated that there is no neutral stability curve, $G_\theta \geqslant 1$ generally implies that the boundary layer is unstable.

Görtler instability is at the root of several physical phenomena with technological applications, such as heat transfer on gas turbine blades [2] or premature transition to turbulence of flows on laminar profiles of new generation (LFC) [3]. Longitudinal vortex structures can occur directly in a boundary layer by different physical mechanisms such as Görtler instability (counter-rotating) or cross-flow instability (co-rotating). The existence of longitudinal vortices in a boundary layer on a concave wall was predicted by Görtler [4]. Blackwelder [5] showed the analogy between the striations present in the wall region of a turbulent boundary layer and the Görtler vortices. In this context Görtler instability provides a fundamental generic flow for studying flows in the presence of longitudinal vorticity. Some preliminary observations of Chomaz and Perrier [6] and Chomaz [7] of Görtler flow on a concave wall provide evidence for the nonlinear convective nature of the instability, in qualitative agreement with the theoretical study of Park and Huerre [8]. The relevant feature is the sensitivity of the instability to the amplitude of the initial perturbations. Görtler vortices cannot be detected at zero forcing. Nonetheless, the application of a localized steady excitation close to the origin of the flow gives rise

* Corresponding author. Tel.: +33-2-40-68-31-39; fax: +33-2-40-68-31-41.
E-mail address: hassan.peerhossaini@polytech.univ-nantes.fr (H. Peerhossaini).

0017-9310/$ - see front matter © 2004 Elsevier Ltd. All rights reserved.
doi:10.1016/j.ijheatmasstransfer.2004.04.006

Nomenclature

C_p	heat capacity $\left(\frac{\mathrm{J}}{\mathrm{kg.K}}\right)$
d_w	wire diameter (m)
G_θ	Görtler number $\left(\frac{U_n\theta}{\upsilon}\sqrt{\frac{\theta}{R}}\right)$
H	height of the counter wall, $H = 0.15$ (m)
Nu	local Nusselt number $Nu = \frac{\varphi_p x}{\lambda \Delta T}$
Pr	Prandtl number, $Pr = \frac{\upsilon}{K}$
R	wall radius of curvature (m)
Re	Reynolds number $\left(\frac{U_n x}{\upsilon}\right)$
St	Stanton number $\left(\frac{\varphi_w}{\rho C_p U_{pw}(T_{wall} - T_\infty)}\right)$
T_f	film temperature, $T_f = \frac{(T_p + T_\infty)}{2}$ (K)
T_∞ or T_{inf}	free stream temperature (K)
T_w	wall temperature (K)
U	Longitudinal component of velocity (m/s)
U_n	free stream velocity or nominal velocity (m/s)
U_{pw}	potential wall velocity, $U_{pw} = \frac{U_n}{\frac{R}{H}\ln(1-\frac{H}{R})} \approx 0.88\ U_n$ (m/s)
x	streamwise direction (m)
y	normal to the wall direction (m)
z	spanwise direction (m)
α	wavenumber
K	thermal diffusivity $\left(\frac{\mathrm{m}^2}{\mathrm{s}}\right)$
υ	kinematic viscosity (m^2/s)
ρ	density (kg/m^3)
φ_w	wall heat flux (W/m^2)
φ_L	heat flux loss (W/m^2)
θ	Blasius momentum thickness $\theta = 0.664x(Re)^{-1/2}$ (m)

to a spatially growing perturbation for forcing amplitudes above a definite threshold.

Another important characteristic of an instability developing in an open flow is its receptivity to initial perturbations, in other words, the absolute or convective aspect of the instability. It is generally agreed that instabilities in open flows are often convective and can become absolute after a second threshold. The primary Görtler instability is considered a convective instability [8].

Streamwise evolution of the vortices was studied by using longitudinal velocity measurements in the y–z plane [9]. The need to follow the spatial development of the vortices is a consequence of the open-system nature of Görtler instability. Unlike Taylor–Couette instability, where the disturbances are confined between two concentric cylinders, boundary-layer disturbances that enter the flow are convected out of it and leave the system. Behind this intuitive insight is in fact a more fundamental notion of convective or absolute instabilities. In a very schematic way, one can say that a flow is convectively unstable if the energy of the initial disturbances is propagated more quickly than it is produced. In other words, a periodic-steady disturbance, in a convectively unstable flow, must be maintained by external sources. Freestream fluctuations in a wind tunnel can constitute precisely such disturbance sources. For absolute, the disturbances need not be maintained by external sources necessary since the temporal amplification of the disturbances is sufficient to contaminate the flow [10].

More generally, determination of the convective or absolute character of the instability makes it possible to privilege a spatial-global or temporal-local step. This has particular practical importance since, according to Huerre and Monkewitz [11], the introduction of a probe into an absolutely unstable flow such as Taylor–Couette instability or Rayleigh–Bénard convection can be the origin of disturbances whose amplification can contaminate the whole flow. Park and Huerre [8] studied primary and secondary instabilities in an asymptotic suction boundary layer on a concave wall and showed that it is in fact a convective instability. Therefore, experimental investigation of this instability must take into account the spatial evolution of the vortices. Petitjeans [12] carried out two types of experiment: a local type that entailed varying freestream velocity and measuring velocity distribution in a normal section at a fixed position x, and a second series that let him follow the evolution of the vortices by maintaining the flow freestream velocity constant. These experiments showed that the results can differ for given Görtler wavenumbers. Due to the convective nature of Görtler flow, we have opted to privilege the spatial step and follow the longitudinal evolution of the vortices.

In Görtler flow, the stability diagram (Fig. 1) is an important guide for experimental measurements in developing boundary layers [1,13,14]. The Görtler number G_θ can be written in the form $G_\theta = \Lambda_\alpha(\theta\alpha)^{3/2}$, where α is the spanwise wavenumber and $\Lambda_\alpha = Re_R(\alpha R)^{-3/2}$, where $Re_R = \frac{U_n R}{\upsilon}$ is the curvature Reynolds number. In a given experiment, for a fixed constant observed wavenumber, the local Görtler number increases as $\theta^{3/2}$ and the coefficient Λ_α is a constant characterizing that particular experiment in the $(G_\theta, (\alpha\theta))$ plane [14]. However, Swearingen and Blackwelder [14] define the coefficient Λ using the

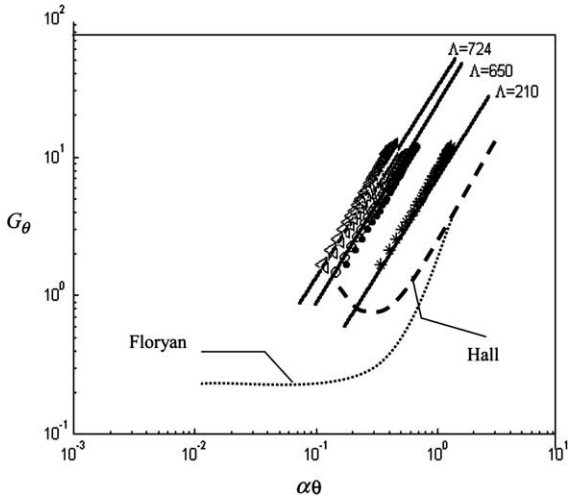

Fig. 1. Different experimental results superposed on the stability diagram. Experimental domains shown by constant Λ lines for the present work: (Δ)$U_n = 4.8$ m/s, $\lambda = 1.5$ mm; ($\bigcirc$) $U_n = 3$ m/s, $\lambda = 2$ cm; Swearingen and Blackwelder ($\bullet$) and; Bippes ($*$). Floryan and Hall marginal stability curves are also shown.

wavelength $\lambda = \frac{2\pi}{\alpha}$, so that $\Lambda_\lambda = Re_R\left(\frac{\lambda}{R}\right)^{3/2}$. Although statistically their experiments gave $\lambda \approx 23$ mm (corresponding to $\Lambda_\lambda \approx 650$), the definite quantitative data to which Sabry and Liu [15] numerical results agreed was $\lambda \approx 18$ mm, which $\Lambda_\lambda \approx 460$. Experiments of Bippes [16] and of Aihara and Koyama [17,18] fall on $\Lambda_\lambda \approx 210$ and $\Lambda_\lambda \approx 235$, respectively. The initial Görtler instabilities observed in the above-mentioned experiments occur, without exception, in the 'amplified region' (nonlinear) of the stability diagram and follow constant Λ_α or Λ_λ lines. Fig. 1 superposes different experimental results on the stability diagram, and Table 1 summarizes the values of Λ for different experimental configurations studied here. We define the coefficient Λ using the wavelength, so that $\Lambda_\lambda = \frac{U_n R}{\upsilon}\left(\frac{\lambda/2}{R}\right)^{3/2}$.

An overview of the effects of Görtler instability on heat transfer is given by Peerhossaini [19]. In the present work, we report on measurements of wall temperature field in the presence of longitudinal vortices forced by an array of wires vertically fixed upstream of a concave boundary layer. By varying the distance between the forcing wires we controlled the wavelength of the longitudinal vortices propagated in the curved boundary layer under the effect of Görtler instability.

The aim of the present work is to provide a method of global analysis to help in the prediction of heat transfer in a boundary layer over a concave surface. Results show that Stanton and Görtler numbers based on theoretical potential wall velocity U_{pw} and Blasius momentum thickness θ on a flat plate are as useful as these numbers calculated based on the real local values of θ and U_{pw}, which need extensive measurement. Boundary-layer sensitivity to various steady perturbations is also studied through heat-transfer enhancement by the vortices and their effect on the transition to turbulence.

2. Experimental apparatus and methods

2.1. Experimental rig and measurement techniques

This study was carried out in a wind tunnel of suction type with freestream turbulence intensity less than 0.7%. The model used (Fig. 2) is composed of a thick leading edge of half a NACA-0024 airfoil, a concave part with radius of curvature 65 cm, a convex part with radius of curvature 15 cm, and a flat-plate trailing edge. The present study used only the concave part of the model, where the Görtler instability occurs. More details on the wind tunnel and concave–convex model used in this work can be found in Peerhossaini and Bahri [20]. In presenting the results, the origin of the longitudinal

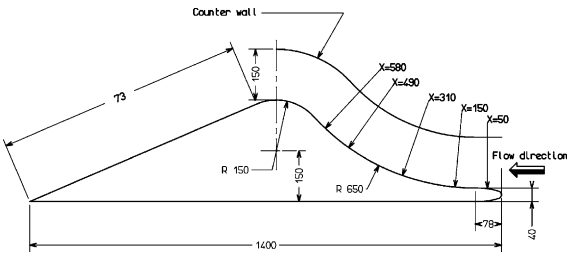

Fig. 2. Schematic diagram of the model (dimensions in mm).

Table 1
Values of Λ for different experimental configurations in the present work

U (m/s)	λ (mm)						
	2.5	5	10	15	20	25	30
2	20	58	164	301	465	649	854
3	31	87	246	453	697	974	1280
4.8	49	139	394	724	1115	1558	2049
7	72	203	575	1056	1626	2273	2988

curvilinear coordinate x is taken at the stagnation line of the leading edge.

The initial disturbances are generated by means of perturbation grids made up of a series of forcing wires of diameter 0.18 mm or 0.80 mm and with 5, 10, 20, 30, 40, 50, and 60 mm spanwise wavelength. The grid is placed vertically 4 mm upstream of the leading edge. The principal role of this perturbation grid is to fix the distance between vortices and their spanwise positions. The model wall is heated with a constant heat flux $\varphi_p = 200$ W/m^2 using double-layered resistive sheets of 130 μm thickness. The heated surface begins at the leading edge and ends at the end of the convex part. The upper layer of the heating sheet in contact with the fluid is a film of constantan of 70 μm thickness heated by the Joule effect. Its lower layer, of thickness 60 μm, is of kapton so as to assure electric isolation of the back face of the heating film. The double-layered heater is fixed on the model wall by a double-faced adhesive that resists temperatures above 100 °C. One hundred and ninety chromel–alumel-type thermocouples of 80 μm diameter were embedded in the double-faced adhesive tape so that their beads are in contact with the kapton part of the heating sheet. Thermocouples are placed in such a way (Fig. 3) that the longitudinal evolution of the wall temperature can be followed as well as its spanwise variation at several longitudinal positions. Thermocouple signal acquisition was carried out by a Keythley K-199 microvoltmeter.

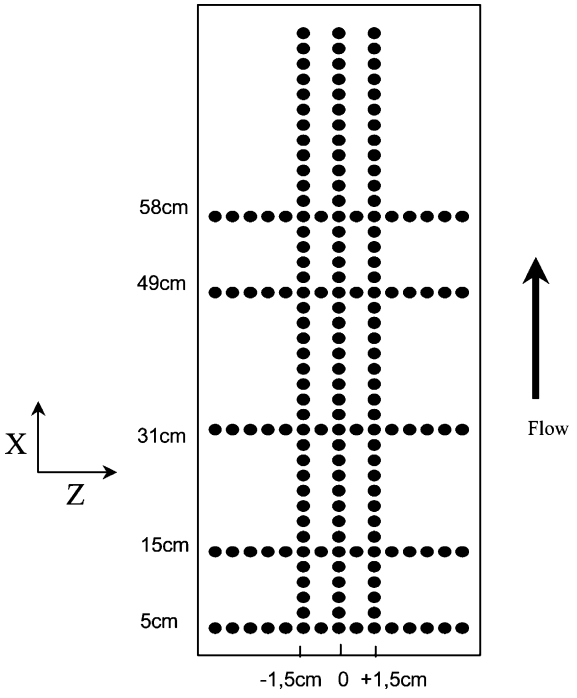

Fig. 3. Position of the thermocouples embedded in the concave wall.

The special geometry of the model causes a nonuniform heat loss from the back of the concave–convex wall that varies with x. To minimize this heat loss, the concave–convex wall was isolated from behind by 3 cm thick phenolic foam ($k = 0.02$ W/m K). The back-wall heat-loss flux was measured by four thermocouples placed in the foam at four streamwise distances. Heat loss varied between 6 and 7 W/m^2, which is between 3% and 3.5% of the constant heat flux delivered by the electric resistive heating sheet. Fig. 4 shows the heat loss percentage as a function of x. The small thickness of the resistive film, its high thermal conductivity (on the order of 0.4 W/m K) and the heat losses below 8 W/m^2 result in temperature differences less than 0.01 °C between the measured temperature and the real temperature of the wall.

Three lines of 40 thermocouples each let us follow the evolution of the temperature field in the flow direction. The spanwise distance between the three rows is 1.5 cm. In order to investigate the spanwise distribution of the wall temperature (upwash and downwash zones) at given axial positions, rows of 15 thermocouples are also implanted in the spanwise direction at downstream positions $x = 5$, 15, 31, 49 and 58 cm. The Stanton number is obtained from wall temperature measurements. The perturbation grid was designed and positioned so that the thermocouple lines coincided with two upwash zones situated at $z = -1.5$ cm and $z = +1.5$ cm and one downwash zone situated at $z = 0$ cm (symmetry line).

Fig. 5 plots the spanwise distribution of wall temperature for the five streamwise distances. At $x = 5$ cm, under flow acceleration caused by the model nose, the values of $T_{wall} - T_{inf}$ (°C) are small, as are their spanwise variations. At $x = 15$ and 31 cm the boundary layer is

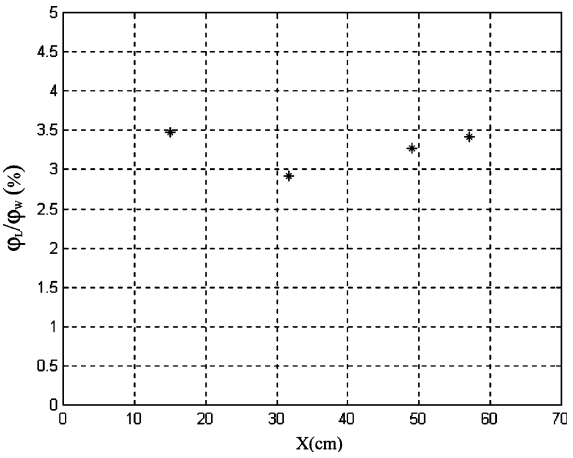

Fig. 4. Percentage of heat loss by conduction from the back of the concave–convex wall plotted as a function of axial position for $U_n = 4.8$ m/s, $d_w = 0$ and $\varphi_p = 200$ W/m^2.

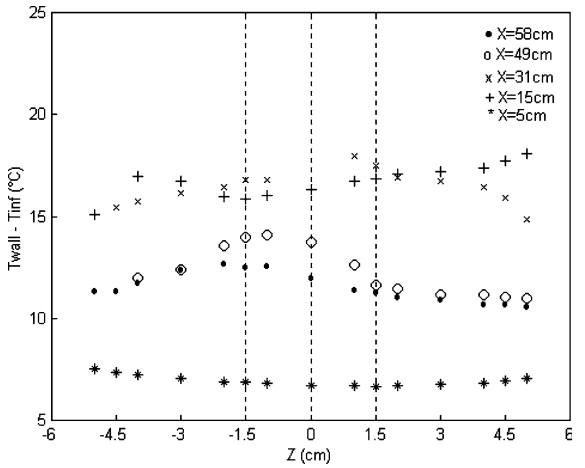

Fig. 5. Spanwise distribution of the wall temperature at five streamwise positions for $U_n = 4.8$ m/s, $d_w = 0$, and $\varphi_p = 200$ W/m^2.

already formed but unsteadiness and turbulence have not yet set in. From $x = 49$ cm the boundary layer becomes unsteady and transition starts, so that the wall temperature decreases.

Fig. 6 shows the evolution of the Stanton number obtained with the wall temperature measured by the three thermocouple lines at $z = -1.5$, 0, +1.5 cm. It is clear that they follow similar evolutions.

Flow velocity was measured by a Pitot tube. Due to the streamline curvature of the concave wall, the characteristic velocity is the wall potential velocity U_{pw} rather than the freestream velocity U_n. The wall potential velocity is defined as $U_{pw} = \frac{U_n}{\frac{R}{H}\ln(1-\frac{H}{R})}$, where H is the height of the counter wall and R the concave wall radius

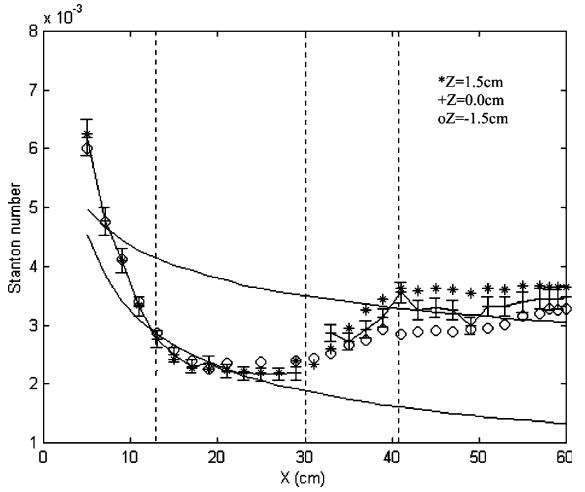

Fig. 6. Evolution of the Stanton number in the longitudinal direction for $U_n = 4.8$ m/s and different transverse positions Z.

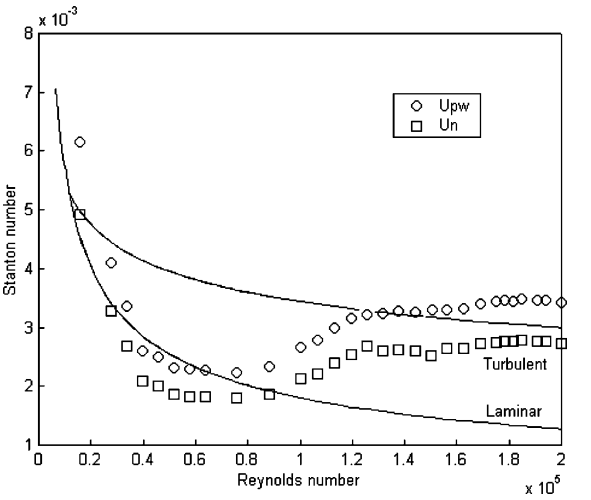

Fig. 7. Choice of the characteristic velocity for Stanton number scaling for $d_w = 0$ and $U_n = 4.8$ m/s.

of curvature ($R > 0$ for concave wall). In the present experiments $U_{pw} \approx 0.88\ U_n$ is obtained theoretically by calculating the potential velocity at $y = 0$ or experimentally by extrapolation to the wall of the experimental points measured outside the boundary layer far from the wall. Fig. 7 shows the variation of the Stanton number with Reynolds number as calculated with U_{pw} and U_n. It can be seen that the U_{pw} curve better matches the correlations in the laminar and turbulent regime. In the rest of this paper U_{pw} is chosen as the scaling velocity for calculation of the Stanton number.

2.2. Dynamical and thermal regimes

Wall heating has destabilizing effects on a boundary-layer flow. First, the increase in the air temperature close to the wall increases the air kinematic viscosity, which causes fluid deceleration close to the wall. This deceleration produces an inflection point in the velocity profile, which is a destabilizing mechanism in a boundary layer [21]. Second, at the same time the air density close to the wall decreases, modifying the gravitational force compared to isothermal flow and potentially triggering a thermo-convective instability in the boundary layer. Kamotami et al. [22] give an estimate of the effects of the temperature variation on the flow stability on concave wall. They showed that these effects depend on the ratio of Gr/G_θ^2 and become important for values of this ratio higher than the unity, where Gr is the local Granshoff number based on the boundary-layer thickness and G_θ is the Görtler number:

$$Gr = \frac{g\beta\Delta T}{\upsilon^2} \times \left(\frac{\upsilon x}{U_n}\right)^{3/2}$$

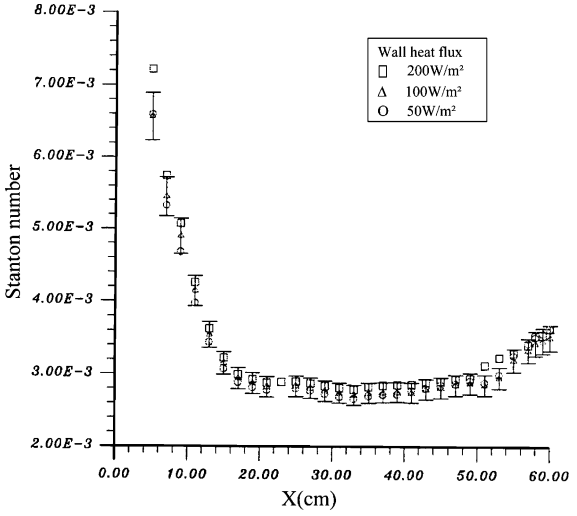

Fig. 8. Longitudinal evolution of the Stanton number according to various densities paritial heat flux for $U_n = 3$ m/s and $Z = 4$ cm.

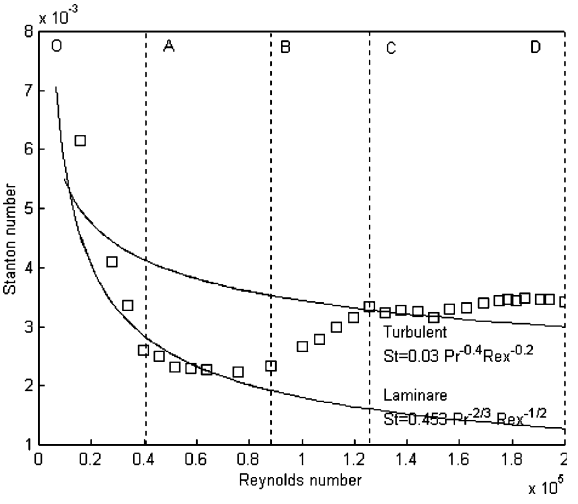

Fig. 9. Evolution of the Stanton number versus Reynolds number for $U_n = 4.8$ m/s in the absence of the vortex-triggering grid.

and

$$G_\theta = \frac{U_n \delta}{\upsilon}\sqrt{\frac{\delta}{R}} \quad \text{with } \delta = \sqrt{\frac{\upsilon x}{U_n}}$$

In the present experiment (at $x = 30$ cm, $\Delta T = 15.5$ °K, $U_n = 4.8$ m/s), the value of this criterion is well below 1 ($Gr/G_\theta^2 = 0.015$). Therefore wall heating does not play a dominant role in flow destabilization. This fact is confirmed in Fig. 8, where one can observe that heating the wall with different values of heat flux, does not affect the longitudinal evolution of the heat transfer coefficient. Even with a fourfold increase in the wall heat flux, the variation in the Stanton number remains below measurement accuracy (5%).

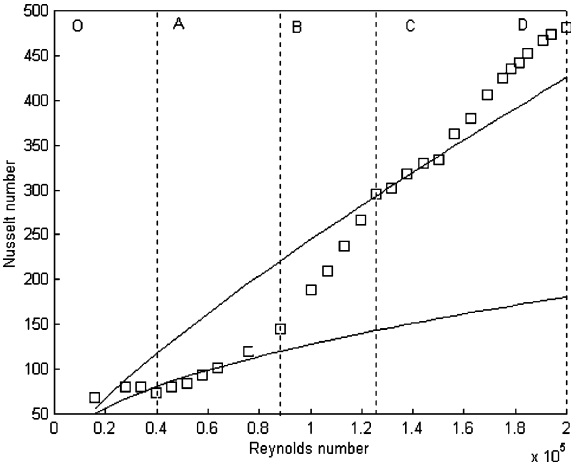

Fig. 10. Evolution of the Nusselt number versus Reynolds number for $U_n = 4.8$ m/s in the absence of the vortex-triggering grid.

3. Results

3.1. Nusselt or Stanton scaling

Wall heat transfer is identified by the Stanton number St, which is calculated from the measured wall temperatures and the wall heat flux. In this section we focus on the evolution of heat transfer on the concave wall. The coefficient of local convective heat transfer between the fluid and the wall can be reduced to either the local Nusselt or Stanton number. Figs. 9 and 10 show the evolution of these two numbers as a function of Reynolds number based on the curvilinear axial position for $U_n = 4.8$ m/s in the absence of the vortex-triggering grid. The experimental results are compared to the correlations for heat transfer on a flat plate [23] in the constant heat flux condition:

- laminar flow: $St = 0.453\,\mathrm{Pr}^{-2/3}\,Re_x^{-1/2}$;
- turbulent flow: $St = 0.03\,\mathrm{Pr}^{-0.4}\,Re_x^{-0.2}$.

These correlations are used as references for the evolution of heat transfer along the concave surface.

Four different stages of the longitudinal evolution of the boundary layer can be distinguished in Figs. 9 and 10:

- *Zone OA*. This zone corresponds to the leading edge and its junction with the concave part. In this zone

Nu and *St* follow approximately the curves corresponding to the laminar boundary layer on the flat plate (2D steady-laminar flow). Deviation of the first few points is due to flow acceleration at the leading edge.

- *Zone AB*. Here heat transfer on the concave wall deviates gradually from the flat plate with the appearance of a "plateau" with roughly constant Stanton number. This heat-transfer intensification is related to the growth of the Görtler vortices under the effect of centrifugal instability (3D steady-laminar flow).
- *Zone BC*. The heat transfer coefficient gradually reaches values close to or above the turbulent boundary layer values on a flat plate. This rapid increase of the heat transfer coefficient (*St* or *Nu*) is due to the appearance of the secondary instability of the Görtler vortices [24]. Indeed, once the Görtler vortices reach a sufficient strength, the subsequent longitudinal velocity gradients cause inflection points where shear instability develops (3D unsteady flow); this secondary instability grows rapidly and induces a premature (compared to the flat plate) boundary-layer transition to turbulence.
- *Zone CD*. Heat transfer ceases to increase and follows the flat-plate turbulent curve. It has been observed [25] that turbulent spots are present in the boundary layer at these Görtler numbers. As Kestoras and Simon [26] and also Toé et al. [24] have noted, the heat-transfer level of the turbulent boundary layer is higher on the concave wall than on a flat plate. This heat-transfer enhancement in the turbulent regime can be explained by the mechanisms responsible for heat-transfer enhancement in the laminar flow: the primary Görtler instability induces longitudinal vortices that are not completely broken down by transition and thus are still weakly present, even in the mean velocity profiles; the secondary instability induces large-scale coherent vortices in the turbulent flow that are more efficient for transport than the smaller turbulent scales.

Fig. 10 shows the same phenomena as Fig. 9, but the local *Nu* value has a strong dependence on x and therefore its variation with *Re* is marked by proportionality to x. On the other hand, variations of *St* are particularly marked by a minimum value just before the appearance of unsteadiness. Therefore it is more appropriate to use the Stanton number in describing heat transfer in the laminar regime because its evolution allows immediate comprehension of the flow state in various longitudinal positions. Moreover, *St* has the advantage of being analogous to the friction coefficient, i.e. it is physically more interesting than *Nu*. However, present results show that the local *Nu* varies weakly with *Re* in zone OA, so that we could readily estimate the mean value of *Nu* on the concave wall before the appearance of the secondary instabilities.

3.2. Reynolds or Görtler scaling

Fig. 11 shows the variation of *St* as a function of *Re* for various values of nominal velocity. The Reynolds number corresponding to the point *A* at which experimental curves deviate from the laminar flat-plate curve varies for different nominal velocities. Fig. 12, which plots the same curves as a function of G_θ, shows that point *A* (deviation from the laminar flat-plate curve)

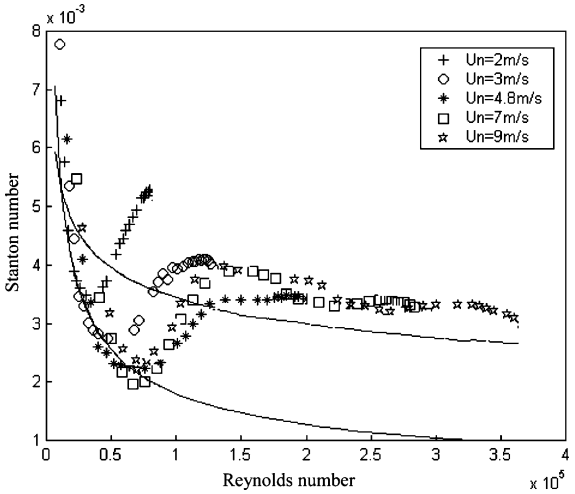

Fig. 11. Evolution of the Stanton number versus Reynolds number for various free-stream velocities in the absence of the vortex-triggering grid.

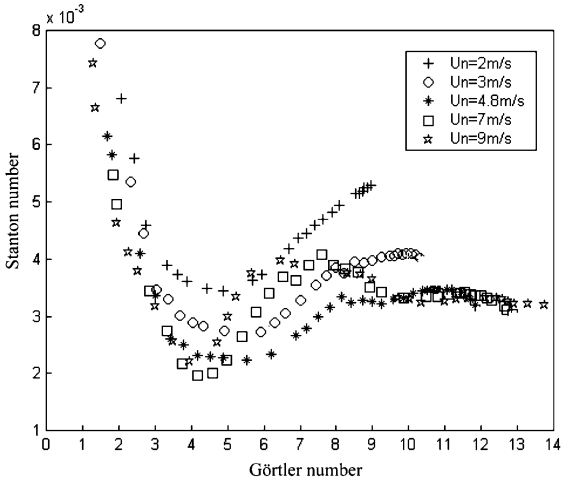

Fig. 12. Evolution of the Stanton number versus Görtler number for various free-stream velocities in the absence of the vortex-triggering grid.

occurs at the same G_θ (i.e. $G_\theta \approx 3.5$) for different nominal velocities. Moreover, the points B where the constant St "plateau" ends also occur at the same value of G_θ for different nominal velocities ($G_\theta \approx 6$). This suggests that in the actual experimental results, G_θ is a better scaling parameter than Re for heat-transfer evolution, so that in this sense the Görtler number is a better similarity parameter than the Reynolds number. Liepmann [27] also observed that the transition to turbulence for different experiments occurred at values of G_θ between 6 and 9, where θ was the spanwise-averaged momentum thickness of the boundary layer. Although G_θ is based on a characteristic Blasius boundary-layer thickness in the present work, the transition was found at around Liepmann's value [27]. For small values of U_n there is a general upward shift, proving that the Stanton and Görtler numbers are not yet the perfect scaling parameters. We describe in detail below the four flow zones outlined above.

3.3. Heat transfer signature of flow regimes

3.3.1. Heat transfer in two-dimensional laminar flow ($G_\theta < 3.5$)

It is observed in Fig. 12 that all curves collapse in their OA part and that points A correspond approximately to the same value of $G_\theta = 3.5$; beyond this G_θ value the curves definitely separate from one another. This separation is more apparent in the St vs. G_θ curves than the St vs. Re curves. For small values of G_θ, the amplitudes of the Görtler vortices are small and they thus have no effect on heat transfer at all. Therefore for $G_\theta < 3.5$, the flat-plate correlation remains valid in the range of parameters studied.

3.3.2. Heat transfer in three-dimensional laminar flow ($3.5 < G_\theta < 6.5$)

In zone AB, the amplitude of the longitudinal vortices becomes significant and the associated disturbances of the velocity and temperature fields become nonlinear, as indicated by Peerhosaini and Bahri [20] and Toé et al. [24]. The result is an increasing deviation of the evolution of St from that of the flat-plate value; for the same value of Re_x heat transfer is increased in the concave boundary layer over two-dimensional (flat-plate) laminar flow. Vorticity growth (vortex intensity) combined with the average increase in δ result in the formation of the "plateaus" AB. On these plateaus the (constant) value of St depends strongly on the U_n; there is neither an explanation of nor a simple law to predict this behaviour. Comparison of Figs. 11 and 12 highlights the fact that, while the Re corresponding to point B varies from curve to curve, the G_θ range for which the plateau occurs is always the same, $3.5 < G_\theta < 6.5$.

3.3.3. Heat transfer in unsteady flow ($6.5 < G_\theta < 9$)

In the BC region, above $G_\theta = 6.5$ the unsteadiness of the flow grows and heat transfer reaches the turbulent level with values sometimes above those for a turbulent boundary layer on a flat plate. While the slopes of the St–Re curves vary in the zone BC, they are always identical on the St–G_θ curves. Moreover, even if the use of the (Blasius) momentum thickness θ in calculating G_θ introduces an error in this three-dimensional flow regime, one obtains roughly the same value of G_θ for all points C, $G_\theta = 9$.

3.3.4. Heat transfer in turbulent flow ($G_\theta > 9$)

As shown in Fig. 12 and observed by Ajakh et al. [25] in hot-wire velocity measurements, the flow can be considered turbulent above $G_\theta > 9$. On the other hand, in the St–Re representation this end of the transition to turbulence does not appear for a unique value of Re. Fig. 11 shows that in the presence of the longitudinal Görtler vortices transition appears earlier (at smaller Reynolds number) for smaller nominal velocities. For $U_n \geqslant 7$ m/s^{-1} the description of the transition to turbulence through the secondary instability of the Görtler vortices must be modified by the fact that transition occurs before the Görtler vortices grow. In an extreme case, for very large U_n, the transitional Reynolds number is attained on the leading edge or on the flat part of the model before any centrifugal effect can become active and therefore, before the vortices develop. Toé et al. [24] found the same St–Re behaviour for $U_n = 7$ and 9 m/s, thus showing that for high velocities the similarity of Re again becomes valid.

In fact, it should be noticed that at high velocities the effect of curvature on heat-transfer enhancement in the laminar and transitional zones is not as significant as at low velocities. Fig. 12 also shows that for $U_n = 7$ m/s, unsteadiness and transition to turbulence start at $G_\theta = 4.5$, which is below the value of 6.5 [24] necessary for the occurrence of secondary Görtler instabilities. On the other hand, for lower velocities the Görtler centrifugal instability develops with the resulting longitudinal vortices that destabilize and induce a premature transition to turbulence in terms of Re. The results in Fig. 11 confirm that globally G_θ lets us follow these phenomena.

3.4. Effects of upstream disturbances

Several studies have shown that the wavelength selection of the primary Görtler instability λ_z depends on the upstream flow conditions. Bradshaw [28] showed that the wavelength could be modified by the last grid in the settling chamber. A systematic experimental study of different disturbance-generator configurations carried out by Kottke [29,30] shows that the vortex wavelength depends directly on the distance between the disturbance generators and the entry of the flow into the unstable

zone. Petitjeans [12] controlled vortex wavelength by regularly spaced cross-flow jets. Swearingen and Blackwelder [14] observed that the replacement or rotation by 90° of the last grid in the settling chamber modified both the relative position and the wavelength of the vortices. It should be noted that $\lambda_z = 23$ mm in their experiments is an average value obtained by spectral analysis.

Swearingen and Blackwelder's [14] results were used in validating several numerical studies. Sabry and Liu [15] and Liu and Lee [31] showed numerically that the value of λ_z agreeing with experimental results is 18 mm. The same value was used by Liu and Domaradzki [32] in a direct numerical simulation of the transition in temporal Görtler problem; their results show good agreement with those of Swearingen and Blackwelder [14]. Therefore, the statistical averaged 23 mm wavelength seems to have no real physical significance. Indeed, since λ_z is a local parameter, it is more clear if it is forced externally rather than letting it be imposed by the settling chamber grids or other uncontrolled perturbations. Thus the precise forced perturbation in the present experiments gives more accurate control of the upstream flow conditions. The several disturbance grids used were made up of two series of wires 0.18 or 0.80 mm in diameter; the forcing wavelengths were 5, 10, 20, 30, 40, 50 or 60 mm.

3.4.1. Effects of the wire diameter

Figs. 13 and 14 show the effect of wire diameter on the Stanton number versus Görtler and Reynolds number for $U_n = 4.8$ m/s. The wire wavelength is 30 mm and the grid is placed vertically 4 mm upstream of the model leading edge. Correlations for laminar and turbulent boundary layers on a flat-plate are also superposed. Three cases are studied: no perturbation grid, 0.18 and 0.80 mm diameter wires. The case without perturbation grid is indicated by $d_w = 0$.

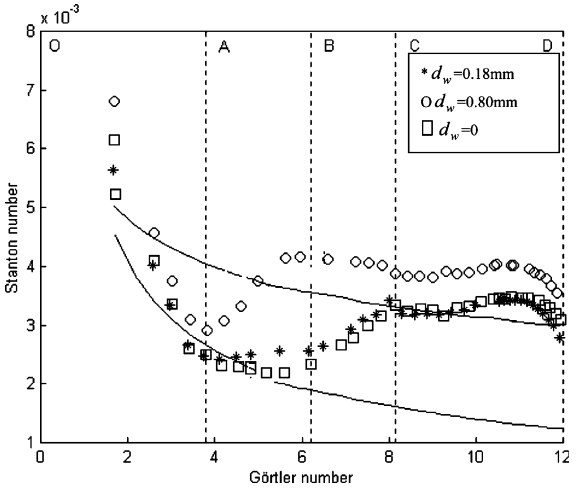

Fig. 13. Effects of wire diameter on the evolution of the Stanton number versus Görtler number for $U_n = 4.8$ m/s, $\lambda_z = 3$ cm.

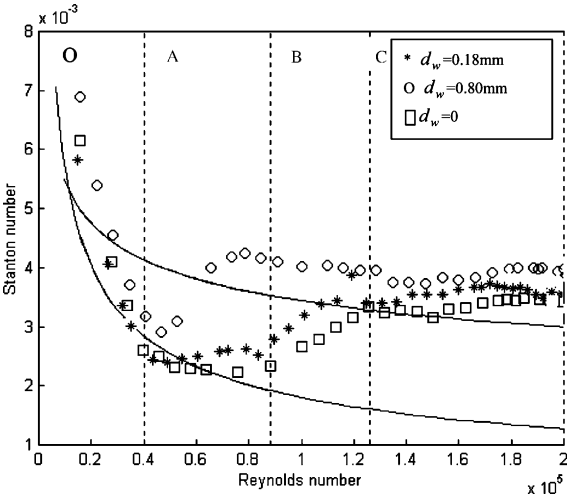

Fig. 14. Effects of wire diameter on the evolution of the Stanton number versus Reynolds number for $U_n = 4.8$ m/s, $\lambda_z = 3$ cm.

The curves of St evolution follow the tendency described in the previous sections. At low Görtler numbers, they follow the laminar flat-plate curve; they deviate from it at $G_\theta \approx 3.8$ ($Re_x \approx 0.45 \times 10^5$) for $d_w = 0.80$ mm, at $G_\theta \approx 4.5$ ($Re_x \approx 0.55 \times 10^5$) for $d_w = 0.18$ mm and at $G_\theta \approx 4.8$ ($Re_x \approx 0.65 \times 10^5$) for $d_w = 0$. A constant Stanton-number plateau then begins to develop that reflects heat-transfer enhancement by Görtler vortices for $d_w = 0$ and 0.18 mm. The end of the plateau corresponds to the state in which the vortices start to become time-dependent. The Stanton number increases under the effect of vortex meandering until it reaches the turbulent boundary layer curve, where the vortex structure has broken down and turbulence has set in. Beyond this point the experimental results follow the trend of the turbulent flat-plate curve.

If the model wall surface were longer, one would expect the curve of Stanton number to relax towards that of the turbulent flat-plate boundary layer. The maximum augmentation (compared to the laminar flat-plate boundary layer) of the Stanton number occurs for $d_w = 0.18$ mm at the end of the characteristic plateau ($G_\theta \approx 6$) where the vortices are fully developed.

For $d_w = 0.80$ mm the transition development scenario is different. As shown in Figs. 13 and 14, the plateau of constant Stanton number does not appear at all. The experimental points follow the laminar flat plate curve up to $G_\theta \approx 3.8$ ($Re_x \approx 0.45 \times 10^5$), then deviate from it and rapidly increase to join the turbulent

flat-plate curve. This fast transition suggests that bypass transition occurs here. However, for the two types of perturbation grid, once the flow has become fully turbulent, it follows the trend of the turbulent flat-plate boundary layer with a slightly higher Stanton number.

3.4.2. Wavelength effect

Fig. 15 shows the evolution of the Stanton number versus Reynolds number with $U_n = 4.8$ m/s for various $\lambda_z = 5$, 10, 20, 30, 40, 50, 60 mm and $d_w = 0.18$ mm and also without perturbation grid. At low Reynolds numbers, all experimental points follow the laminar flat-plate curve. They depart from it at $Re_x = 0.45 \times 10^5$ ($G_\theta \approx 3.8$) for $\lambda_z = 5$ mm, $\lambda_z = 10$ mm and $\lambda_z = 20$ mm ($\lambda_z \leqslant 20$ mm). However, for $\lambda_z > 20$ mm this deviation occurs at $Re_x = 0.55 \times 10^5$ ($G_\theta \approx 4.5$) and a uniform-Stanton-number plateau starts to appear, illustrating heat-transfer enhancement by Görtler vortices.

These two different types of evolution should be interpreted as a consequence of wavelength. At large wavelengths the perturbations induced by the grid are weak and the generated Görtler vortices do not significantly modify the transition to turbulence described in Section 3.1. However, for $\lambda_z \leqslant 20$ mm, the spatial density of the input perturbation seems to go beyond a critical value and imposes a direct transition to turbulence. For these high-perturbation cases, the transition can be considered a bypass transition and heat transfer increases with the perturbation increase (λ_z decrease).

The highest increase (compared to the laminar flat-plate boundary layer) in Stanton number appears for the three lowest spanwise wavelengths, at the end of the transition zone. If the flow is perturbed by a large d_w and small λ_z grid, it is evident that bypass transition will occur, as shown in Fig. 16. It is interesting to note in this figure that vortices with wavelength less than $\lambda_z = 30$ mm advance the transition to turbulence compared with those of $\lambda_z \geqslant 30$ mm. This can be attributed to the sensitivity of the bypass transition to the level of the upstream perturbations or turbulent intensity [33]. One notices, however, that for $\lambda_z = 5$ mm, from the beginning the Stanton number follows the trend of the curve for a turbulent flat-plate boundary layer but at a much higher Stanton number value.

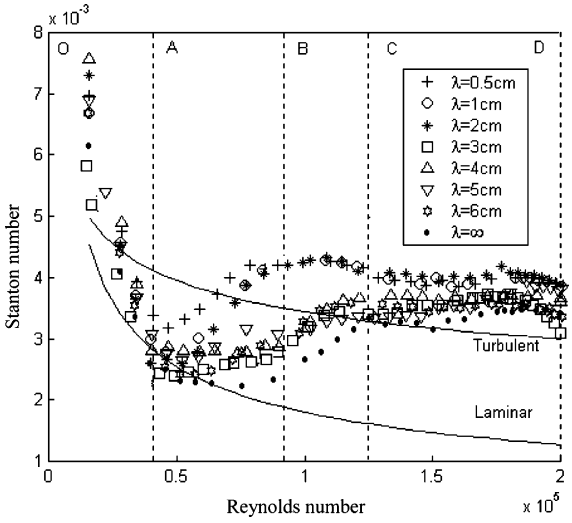

Fig. 15. Effects of forcing wavelength on the evolution of the Stanton number versus Reynolds number for $U_n = 4.8$ m/s and $d_w = 0.18$ mm.

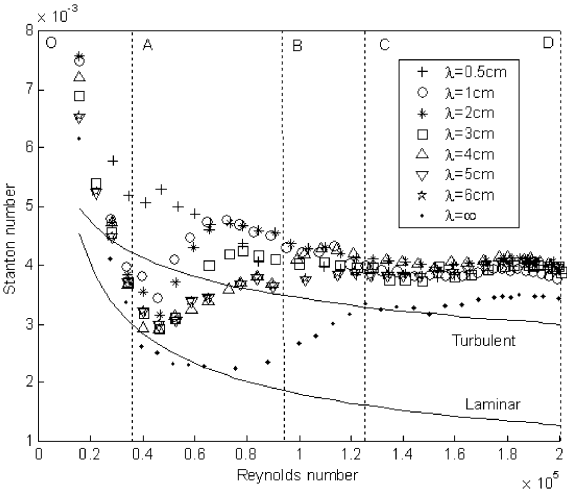

Fig. 16. Effects of forcing wavelength on the evolution of the Stanton number versus Reynolds number for $U_n = 4.8$ m/s and $d_w = 0.80$ mm.

The effects of forcing wavelength expressed in terms of maximum Stanton number increase (%) are compared with the no-perturbation-grid case in Table 2. Table 3 shows the values of transitional Reynolds number and Görtler number with different experimental configurations (wavelength and wire diameter) in the present work and for $U_n = 4.8$ m/s. More details of the wavelength effects on heat transfer enhancement can be found in [34].

Table 2
Effects of forcing wavelength expressed in terms of maximum Stanton number increase (%) compared with no perturbation grid case

λ (mm)	5	10	20	30
St	41% ($G_\theta = 4.2$)	20% ($G_\theta = 4.5$)	15% ($G_\theta = 5$)	10% ($G_\theta = 6.5$)

Table 3
Values of transitional Reynolds number and Görtler number with different experimental configuration in the present work and for $U_n = 4.8$ m/s

d_w (mm)	λ (mm)					
	5	10	20	30	40	600 mm
0.18	$Re_x \approx 0.45 \times 10^5$	$Re_x \approx 0.45 \times 10^5$	$Re_x \approx 0.45 \times 10^5$	$Re_x \approx 0.55 \times 10^5$	$Re_x \approx 0.55 \times 10^5$	$Re_x \approx 0.55 \times 10^5$
	$G_\theta \approx 3.8$	$G_\theta \approx 3.8$	$G_\theta \approx 3.8$	$G_\theta \approx 4.5$	$G_\theta \approx 4.5$	$G_\theta \approx 4.5$
0.80	$Re_x \approx 0.41 \times 10^5$	$Re_x \approx 0.45 \times 10^5$	$Re_x \approx 0.45 \times 10^5$	$Re_x \approx 0.45 \times 10^5$	$Re_x \approx 0.45 \times 10^5$	$Re_x \approx 0.45 \times 10^5$
	$G_\theta \approx 3.4$	$G_\theta \approx 3.8$	$G_\theta \approx 3.8$	$G_\theta \approx 3.8$	$G_\theta \approx 3.8$	$G_\theta \approx 3.8$

4. Concluding remarks and discussion

Experiments under well-controlled conditions were carried out on a concave heated wall in order to understand the effects of Görtler instability and its transition to turbulence on heat transfer from the wall to the boundary layer. Another aim was to obtain reliable data and pertinent dimensionless parameters to scale the heat-transfer problem most appropriately. Since the streamwise evolution of heat transfer under the effects of streamwise vorticity was of special interest, in these experiments (unlike those in [24,25]), time-averaged wall temperature was used as the signature of the Görtler vortices. Thus the longitudinal evolution of heat transfer expressed in terms of conventional Nusselt number and the Stanton number was related to the axial evolution of the Görtler vortices. In heat transfer analysis, it is customary to use the Nusselt or the Stanton number without distinction. The present work shows, however, that the Stanton number reflects more directly than the Nusselt number the effects of longitudinal vorticity on heat transfer. In the same manner, the Görtler number scales the flow reasonably, while the Reynolds number does not. Thus the Görtler number emerges as the natural control parameter from the Navier–Stokes equations written in curvilinear coordinates for the analysis of Görtler stability.

Nonetheless, as has been argued theoretically by Hall [1] and shown experimentally, the notion of a unique marginal stability curve, so common in stability analysis, is not valid for Görtler stability. The critical value of the Görtler number G_θ depends on where and how upstream perturbations were generated before entering the boundary layer. This raises questions about the fundamental pertinence of the Görtler number as the scaling parameter and its preference to the simple Reynolds number. The present work, from the study of a large number of experimental cases, concluded that the Görtler number predicts satisfactorily the different stages of Görtler stability:

- primary Görtler instability appears for $G_\theta > 3.5$;
- secondary Görtler instability occurs for $G_\theta > 6.5$;
- transition to turbulence is accomplished for $G_\theta > 9$.

Nevertheless, Fig. 12 shows that experimental curves do not collapse in the St–G_θ plane, suggesting that these two dimensionless parameters are still not the perfect ideal scaling parameters.

At this stage there exists no clear clue to such ideal parameters. This difficulty can be attributed to the fact that the convectional definition of the Stanton number is not adapted to the flows with coherent structures such as Görtler vortices. This definition takes into consideration neither the spanwise components of the velocity nor its upwash and downwash components, which contribute

much to the enhancement of heat transfer from the wall. To these one can add the time dependence of the axial velocity due to the higher modes of instability. To take these effects into account, one can introduce into the Stanton number an "effective" velocity U_{eff} defined as

$$U_{\text{eff}} = U_{\text{pw}} + a\vec{v} + bu'_{\text{rms}}$$

where v is the spanwise and upwash or downwash components, u'_{rms} is the time-dependent components, and a and b are constants to be evaluated experimentally. This hypothesis needs to be studied in more detail.

It was also shown that correlations for the prediction of Stanton number on a flat plate in laminar region work quite well for a concave wall if G_θ does not exceed 3.5. In a concave boundary layer, transition can occur through different mechanisms. If transition is triggered by Görtler instability, it is characterized in the St–G_θ plane by a constant Stanton-number plateau where heat-transfer enhancement by the vortices balances the heat-transfer reduction due to the boundary-layer thickening (corresponding to zone AB in Fig. 9). However, the Reynolds number can reach a critical value around 0.65×10^5 before the Görtler number increases above 3.5. In this case (for example $U_{\text{n}} > 7\ \text{m s}^{-1}$ in Fig. 11), transition is not by Görtler instability, as Toé et al. [24] found. Experiments have shown that many flows, including boundary-layer flows, may undergo transition to turbulence at low Reynolds numbers, well below the critical value from the linear stability theory. This transition mechanism, named "bypass transition" in 1969 by Morkovin [33], implies that "we can bypass the Tollmien–Schlichting (or other mechanisms) altogether". Ellingsen and Palm [35] considered the inviscid evolution of an initial disturbance independent of the streamwise coordinate and proposed a mechanism according to which streamwise velocity may grow linearly in time and produce alternating high- and low-velocity streaks. It was later shown by Schmidt and Henningson [36] through the linearized Navier–Stokes equations that significant transient growth may occur before the exponential growth of the perturbation induces transition. Such transient growth is larger for disturbances that are periodic in the spanwise direction; it can exist for subcritical values of Reynolds number and is the mechanism underlying the bypass transition. In the case of a concave wall, weak spanwise periodic perturbations that have not been able to evolve to Görtler vortices (due to insufficient G_θ value) thus contribute to the occurrence of the bypass transition and significantly increase the heat transfer from the wall.

References

[1] P. Hall, The linear development of Görtler vortices in growing boundary layer, J. Fluid Mech. 130 (1983) 41–58.

[2] H. Peerhossaini, J.E. Wesfreid, Les tourbillons de Görtler et leurs influence sur les turbines à gaz, Bull Assoc. Tech. Maritime Aéronaut. 88 (1988) 361–381.

[3] S.H. Tim, L.R. Helen, S.S. William, CFD validation issues in transition modeling, in: Proceedings of the 27th AIAA Fluid Dynamics Conference, 1996.

[4] H. Görtler, On the three-dimensional instability of laminar boundary layers on Concave Walls, Nacher. Ges. Wiss. Göttingen 2, (NACA TM 1375, 1954) 1–26.

[5] R.F. Blackwelder, Analogies between transitional and turbulent boundary layers, Phys. Fluids 26 (10) (1983) 2807–2815.

[6] J.M. Chomaz, M. Perrier, in: J.E. Jimenez (Ed.), The Geometry of Turbulence, NATO ASI Series B, Plenum, New York, 1991.

[7] J.M. Chomaz, Absolute and convective instabilities in nonlinear systems, Phys. Rev. Lett. 69 (13) (1992) 1931–1934.

[8] D.S. Park, P. Huerre, Primary and secondary instabilities of the asymptotic suction boundary layer on a curved plate, J. Fluid Mech. 283 (1995) 249–272.

[9] A. Ajakh, Etude expérimentale de l'instabilité de Görtler: identification de critères d'amplification et de l'intermittence: effets de bord d'attaque et de forçage de longueur d'onde, Ph.D. dissertation, University of Nantes, France 1997.

[10] P.A. Monkewitz, The role of absolute and convective instability in predicting the behaviour of fluid systems, Eur. J. Mech. B/Fluids 9 (1990) 395–413.

[11] P. Huerre, P.A. Monkewitz, Absolute and convective instabilities in free shear layers, J. Fluid Mech. 159 (1985) 151–168.

[12] P. Petitejeans, Etude expérimentale des instabilités de couche limites sur des paroi concaves: instabilité de Görtler, Ph.D. dissertation, University of Paris 6, France 1992.

[13] J.M. Floryan, W.S. Saric, Stability of Görtler vortices in boundary layers, AIAA J. 20 (1982) 316–324.

[14] J.D. Swearingen, R.F. Blackwelder, The growth and breakdown of streamwise vortices in the presence of a wall, J. Fluid Mech. 182 (1987) 255–290.

[15] A.S. Sabry, J.T.C. Liu, Concentration and heat transfer in nonlinear Görtler vortex flow and the analogy with longitudinal momentum transfer, Proc. R. Soc. London 432 (1991) 1–12.

[16] H. Bippes, Experimental study of the laminar-turbulent transition on a concave wall in a parallel flow, NASA TM 75243, 1972 (1987 translation).

[17] Y. Aihara, H. Koyama, Generation, development and distortion of longitudinal vortices in boundary layers along concave and flat plate, in: H.H. Fernholz, E. Krause (Eds.), Three-Dimensional Turbulent Boundary Layers, Springer, 1982, pp. 210–220.

[18] Y. Aihara, H. Koyama, Nonlinear development and secondary instability of Görtler vortices, in: F.M. Schroeder (Ed.), Stability in Mechanics of Continua, Springer, 1982, pp. 345–352.

[19] H. Peerhossaini, On the effects of streamwise vortices on wall heat transfer, Begell House Publishers, New York, 1997.

[20] H. Peerhossaini, F. Bahri, On the spectral distribution of themodes in nonlinear Görtler instability, Exp. Therm. Fluid Sci. 16 (1998) 195–208.
[21] H. Schliching, Boundary Layer Theory, sixth ed., McGraw-Hill, NewYork, 1968.
[22] Y. Kamotani, J.K. Lin, S. Ostrach, Effect of destabilizing heating on Görtler vortices, J. Heat Transfer 107 (1985) 877–882.
[23] W.M. Kays, M.E. Crawford, Convection Heat and Mass Transfer, Third ed., McGraw-Hill, New York, 1993.
[24] R. Toé, A. Ajakh, H. Peerhossaini, Heat transfer enhancement by Görtler instability, Int. J. Heat Fluid Flow 23 (2002) 194–204.
[25] A. Ajakh, M.D. Kestoras, R. Toé, H. Peerhossaini, Influence of forced perturbations in the stagnation region on Görtler instability, AIAA J. 37 (12) (1999) 1572–1577.
[26] M.D. Kestoras, T.W. Simon, Combined effects of concave curvature and high free-stream turbulence intensity on boundary layer heat momentum transport. ASME Winter Annual Meeting New Oreans, LA, 1993.
[27] H.W. Liepmann, Investigation of boundary layer transition on concave wall, NACA Technical Report, 1945.
[28] P. Bradshaw, Effect of streamline curvature on turbulent flow, AGARDOgraph 169 (1973).
[29] V. Kottke, On the instability of laminar boundary layer along a concave wall towards Görtler vortices, in: J.E. Wesfreid, H. Brand (Eds.), Propagation and Non-equilibrium Systems, Springer, Berlin, 1988.
[30] V. Kottke, Effects of longitudinal vortices on heat and mass transfer, in: Heat Transfer in Single Phase flows, Recent Development and Enhancement, EUROTHERM Seminar 9, Bochum, Germany 1989.
[31] J.T.C. Liu, K. Lee, Heat transfer in a strongly nonlinear spatially developing longitudinal vortices system, Phys. Fluids 7 (3) (1995) 559–599.
[32] W. Liu, J.A. Domaradzki, Direct numerical simulation of transition to turbulence in Görtler flow, J. Fluid Mech. 246 (1993) 209–267.
[33] M.V. Morkovin, Environmental disturbances, instabilities and onset of turbulence in open flows, NATO Advanced Research Workshop on Görtler Vortex Flows, June 11–14, 1990 Nantes, France, p. 1.
[34] L. Momayez, P. Dupont, H. Peerhossaini, Effects of vortex organization on heat transfer enhancement by Görtler instability, Int. J. Therm. Sci. (2004) (in press).
[35] T.A. Ellingsen, E. Palm, Stability of linear flow, J. Fluid Mech. 18 (4) (1974) 487–488.
[36] P.J. Schmidt, D.S. Henningson, Stability and transition in shear flows, Springer, Berlin, 2001.